Draft version August 9, 2022
Typeset using LaTeX **twocolumn** style in AASTeX631

Fast neutrino cooling in the accreting neutron star MXB 1659-29

Melissa Mendes [1], Farrukh J. Fattoyev [2], Andrew Cumming [1] and Charles Gale [3]

[1] *Department of Physics and McGill Space Institute, McGill University, 3600 rue University, Montreal, QC, H3A 2T8, Canada*
[2] *Department of Physics, Manhattan College, Riverdale, New York 10471, USA*
[3] *Department of Physics, McGill University, 3600 rue University, Montreal, QC, H3A 2T8, Canada*

Submitted to ApJ

ABSTRACT

Modelling of crust heating and cooling across multiple accretion outbursts of the low mass X-ray binary MXB 1659-29 indicates that the neutrino luminosity of the neutron star core is consistent with direct Urca reactions occurring in $\sim 1\%$ of the core volume. We investigate this scenario with neutron star models that include a detailed equation of state parametrized by the slope of the nuclear symmetry energy L, and a range of neutron and proton superfluid gaps. We find that the predicted neutron star mass depends sensitively on L and the assumed gaps. We discuss which combinations of superfluid gaps reproduce the inferred neutrino luminosity. Larger values of $L \gtrsim 80$ MeV require superfluidity to suppress dUrca reactions in low mass neutron stars, i.e. that the proton or neutron gap is sufficiently strong and extends to high enough density. However, the largest gaps give masses near the maximum mass, making it difficult to accommodate colder neutron stars. We consider models with reduced dUrca normalization as an approximation of alternative, less efficient, fast cooling processes in exotic cores. We find solutions with a larger emitting volume, providing a more natural explanation for the observed neutrino luminosity, provided the fast cooling process is within a factor of ~ 1000 of dUrca. The heat capacities of our models span the range from fully-paired to fully-unpaired nucleons meaning that long term observations of core cooling could distinguish between models. We discuss the impact of future constraints on neutron star mass, radius and the density dependence of the symmetry energy.

Keywords: X-ray bursts — Neutron stars — Stellar winds

1. INTRODUCTION

Neutron stars in transiently-accreting low mass X-ray binaries (LMXBs) are remarkable laboratories to probe the physics of dense matter (for a review see Wijnands et al. 2017). While accreting, the neutron star crust is heated by accretion-induced nuclear reactions, with most of the energy flowing inwards to the neutron star core. After accretion ends, in the quiescent phase, the neutron star surface temperature can be measured, which in turn gives a measure of the neutron star core temperature. The quiescent temperatures and luminosities of LMXB neutron stars have been used to infer the efficiency of neutrino emission processes and superfluid state in their cores (Yakovlev & Pethick 2004; Heinke et al. 2007; Levenfish & Haensel 2007; Heinke et al. 2009; Wijnands et al. 2013; Beznogov & Yakovlev 2015a,b; Han & Steiner 2017; Potekhin et al. 2019), the thermal conductivity and superfluidity of the neutron star crust (Shternin et al. 2007; Brown & Cumming 2009; Page & Reddy 2012), and the heat capacity of the core (Cumming et al. 2017; Degenaar et al. 2021).

There is growing evidence that a number of neutron stars have highly-efficient fast neutrino processes in their cores, based on very low quiescent temperatures (Heinke et al. 2007, 2009; Han & Steiner 2017; Potekhin et al. 2019). Characterized by a local emissivity $\propto T^6$, where T is the local temperature, the most efficient fast neutrino process is the direct Urca (dUrca) process in nucleonic matter in which neutrinos are produced by the

Corresponding author: Melissa Mendes
melissa.mendessilva@mail.mcgill.ca

reactions (Lattimer et al. 1991)

$$n \to p + e^- + \bar{\nu}_e, \quad p + e^- \to n + \nu_e. \tag{1}$$

Momentum conservation in these reactions means that they can proceed only if the proton fraction is sufficiently large ($Y_p \gtrsim 1/9$). This means that determining that the dUrca process is happening in a neutron star core directly constrains the proton fraction and therefore the value of the nuclear symmetry energy at high density (see discussion in Lattimer 2018). It also means that the central density and therefore mass of the neutron star is large enough to achieve the critical value of Y_p. With more exotic compositions, such as a meson condensate or quark matter, other fast processes are possible, with the same $\propto T^6$ scaling but a typically smaller normalization (see Yakovlev et al. 2001 for a review). The core temperature is therefore a very powerful observable that depends on the unknown composition of neutron star cores.

The LMXB MXB 1659-29 has shown multiple accretion outbursts in which the neutron star crust has been observed to thermally-relax in quiescence (Parikh et al. 2019). This is unusual because most LMXBs with multiple outbursts have short, frequent outbursts that do not significantly heat the crust at depth; while the LMXBs with large outbursts that heat the crust significantly, have typically only shown one outburst because the recurrence time between outbursts is very long. MXB 1659-29 went into outburst in the late 1970s, in 2001 and again in 2015, with each outburst lasting ~ 2 years (Cackett et al. 2006; Parikh et al. 2019).

By modelling the sequence of outbursts in MXB 1659-29 and the relaxation of the surface temperature in quiescence, Brown et al. (2018) showed that the core must be cooled by a fast neutrino process. The rate at which the neutron star cools after each outburst depends on the temperature of the neutron star crust, set by the rate at which the neutron star core is being heated and therefore cooled by neutrinos. The composition of the neutron star envelope is also constrained by the shape of the cooling curve, reducing an uncertainty in mapping the surface temperature to core temperature (Cumming et al. 2017) (for MXB 1659-29, the inferred core temperature is $\approx 2.5 \times 10^7$ K). Slow neutrino processes, *i.e.* less efficient processes such as modified URCA with emissivity $\propto T^8$, cannot provide the required neutrino luminosity at this core temperature.

Computing an average value of L_ν/T^6 for the core and comparing with the expected value for dUrca, (Brown et al. 2018) found that the neutrino cooling luminosity of MXB 1659-29 is consistent with dUrca occurring over about $\sim 1\%$ of the core volume. Such a low effective emitting volume gives an interesting constraint on the neutron star in MXB 1659-29. Possible explanations are that (1) the neutron star has a mass within a few percent of the mass at which dUrca reactions become possible, (2) superfluidity suppresses the dUrca reactions throughout most of the available volume, reducing the overall luminosity, or (3) a less efficient fast process is operating over the core. Brown et al. (2018) pointed out that these possibilities could in principle be distinguished because they make different predictions for the cooling rate of the core in quiescence because the heat capacity of the core depends on its composition and the extent of superfluidity.

In this paper, we explore the different scenarios for the neutrino emission of MXB 1659-29 using detailed neutron star models that include a variety of superfluid gap models. We use an equation of state parametrized by the slope of the nuclear symmetry energy L, since this parameter determines the proton fraction at high density and therefore the onset density for dUrca reactions. We describe the input microphysics that we use in §2. In §3, we investigate the values of L and neutron star mass that are required to reproduce the observed neutrino luminosity of MXB 1659-29 under different assumptions about the superfluid gap. In §4, we relax the assumption that neutrino emission is by dUrca and consider the effect of reducing the normalization of the dUrca rate on the emitting volume fraction and allowed range of neutron star mass. In §5, we calculate the heat capacity of our models since this is a potential observable that can distinguish the different scenarios. We end with a discussion of our results in §6.

2. DETAILS OF THE CALCULATION AND INPUT MICROPHYSICS

2.1. *Equation of state and neutron star structure*

The family of equations of state (EOS) we use to describe the core of neutron stars is based on relativistic mean field (RMF) model FSUGold2 (Chen & Piekarewicz 2014). This EOS was one of the first to reproduce not only ground-state properties of finite nuclei, but also the maximum observed neutron star mass at the time. A detailed framework of the EOS we generate is available in Mendes et al. (2021), but we summarize their main characteristics here, for convenience.

We consider a minimal model in which only neutrons, protons, electrons and muons are the particle constituents of neutron stars. Consider the expansion of the total energy per nucleon $E(\rho, \alpha)$ at zero temperature,

$$E(\rho, \alpha) = E_{\rm SNM}(\rho) + E_{\rm sym}(\rho) \cdot \alpha^2 + \mathcal{O}\left(\alpha^4\right) \tag{2}$$

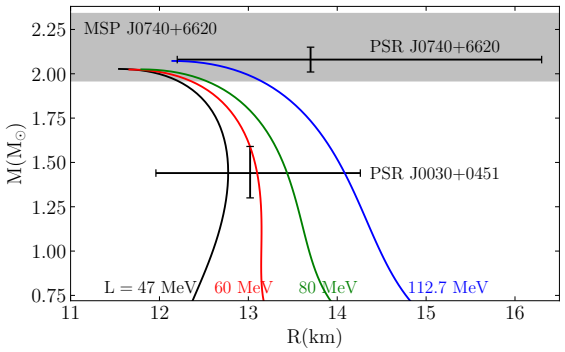

Figure 1. Mass versus radius curves of equations of state with $L = 47$ MeV, $L = 60$ MeV, $L = 80$ MeV and $L = 112.7$ MeV, from left to right. Observational constraints for PSR $J0030+0451$ (Miller et al. 2019) and PSR $J0740+6620$ (Miller et al. 2021) indicated with error bars and maximum mass neutron star observed to date, MSP $J0740+6620$ (Cromartie et al. 2019), with shaded region.

where $\rho = \rho_{\rm n}+\rho_{\rm p}$ is the total baryon number density and $\alpha = (\rho_{\rm n} - \rho_{\rm p})/\rho$ is the neutron-proton asymmetry parameter. Next, consider the Taylor series (Piekarewicz & Centelles 2009) that characterize both the energy per nucleon in symmetric nuclear matter (SNM), $E_{\rm SNM}(\rho)$, and the symmetry energy, $E_{\rm sym}(\rho)$, near the nuclear saturation density $\rho_{\rm sat} = 0.15$ fm^{-3},

$$\begin{aligned} E_{\rm SNM}(\rho) &= B + \frac{1}{2}Kx^2 + \cdots \\ E_{\rm sym}(\rho) &= J + Lx + \frac{1}{2}K_{\rm sym}x^2 + \cdots \\ &\text{where } x = (\rho - \rho_{\rm sat})/3\rho_{\rm sat}. \end{aligned} \tag{3}$$

The family of the EOS we work with shares identical SNM bulk parameters, such as the energy per nucleon $B = -16.26$ MeV and incompressibility coefficient $K = 237.7$ MeV. The symmetry energy $\tilde{J}$ at a subsaturation density of $\rho = 0.1$ fm^{-3} is also fixed to ensure that binding energies and charge radii of finite nuclei are well reproduced. Their different slope of symmetry energy (L), varying from 47 MeV to 112.7 MeV, provide distinct neutron skin thicknesses and neutron star properties, such as radii, all consistent with the current experimental and observational data (Adhikari et al. 2021; Riley et al. 2019; Miller et al. 2019; Abbott et al. 2017, 2018). In particular, increasing L leads to a larger symmetry energy at supersaturation densities, which increases the proton fraction $Y_{\rm p} = \rho_{\rm p}/\rho$ in the innermost region of the star. In addition, increasing L leads to larger neutron star radii. The mass-radius curves for different L values are shown in Figure 1.

The outer crust is described by the EOS from Baym et al. (1971) and the inner crust, by the EOS from Negele & Vautherin (1973). We assume a non-rotating spherically-symmetric neutron star, and solve the Tolman-Oppenheimer-Volkoff (TOV) equations

$$\begin{aligned} \frac{{\rm d}P}{{\rm d}r} &= -\frac{\mathcal{E}(r)}{c^2}\frac{Gm(r)}{r^2}\left[1+\frac{P(r)}{\mathcal{E}(r)}\right] \\ &\quad \left[1+\frac{4\pi r^3 P(r)}{m(r)c^2}\right]\left[1-\frac{2Gm(r)}{c^2 r}\right]^{-1} \\ \frac{{\rm d}m}{{\rm d}r} &= 4\pi r^2 \frac{\mathcal{E}(r)}{c^2} \\ \frac{{\rm d}\phi}{{\rm d}r} &= -\frac{1}{\mathcal{E}(r)+P(r)}\frac{{\rm d}P}{{\rm d}r}, \end{aligned} \tag{4}$$

where $m(r)$ is the mass within radius r, $P(r)$ is the pressure, $\mathcal{E}(r)$ is the energy density and $\phi(r)$ is the gravitational potential such that at the surface of the star, $r = R$ and $m = M$, the pressure vanishes, $P(R) = 0$ and $\phi(R) = \frac{1}{2}\ln(1 - 2GM/c^2R)$, G is the gravitational constant.

2.2. *Neutrino emissivity*

Since our goal is to reproduce the inferred neutrino luminosity of MXB 1659-29, we consider the fast cooling process of dUrca only. If there are no muons participating, dUrca cooling takes place through the reactions in equation (1) which conserve momentum only if

$$k_{Fn} \leq k_{Fp} + k_{Fe}, \tag{5}$$

which implies that for dUrca reactions the proton fraction must exceed a threshold value

$$Y_p \geq Y_{\rm p\,dUrca} = \left[Y_n^{1/3} - Y_e^{1/3}\right]^3, \tag{6}$$

as explained in Yakovlev et al. (2001). Here, $k_{\rm Fx}$ are the Fermi momenta, a function of $\rho_{\rm x}$, the number density for each species and the particle fraction $Y_{\rm x}$. When muons participate, additional dUrca reactions take place

$$n \to p + \mu^- + \bar{\nu}_{\mu^-}, \quad p + \mu^- \to n + \nu_{\mu^-} \tag{7}$$

which has its own threshold given by replacing k_{Fe} with $k_{F\mu}$ in equation (5). As well as introducing an additional neutrino producing reaction, muons also modify the electron fraction $Y_e = Y_p - Y_\mu$ which enters equation (6), and so modify the electron dUrca channel even before the threshold for muon dUrca is reached.

The threshold proton fraction corresponds to a threshold density $\rho_{\rm dUrca}$ for dUrca processes to occur. Only in regions of the core with $\rho > \rho_{\rm dUrca}$ is dUrca allowed, and this also implies that only neutron stars massive enough to have a central density $\rho_c > \rho_{\rm dUrca}$ can cool by dUrca. The dUrca neutrino luminosity, as seen by an observer at infinity, is given by

$$L^{\infty}_{\nu_{\rm dUrca}} = \int_0^{R_{\rm core}} \frac{4\pi r^2 \epsilon_0^{\rm dUrca,total} e^{2\,\phi(r)}}{(1-2Gm(r)/c^2 r)^{1/2}}\,dr, \tag{8}$$

where the integral is over the neutron star core and the local neutrino emissivity is (Yakovlev et al. 2001)

$$\begin{aligned}\epsilon_0^{\mathrm{dUrca},e^-} &= \frac{457\pi}{10080} G_{\mathrm{F}}^2 \cos^2\theta_{\mathrm{C}} \left(1+3g_{\mathrm{A}}^2\right) \\ &\quad \times \frac{m_n^* m_{\mathrm{p}}^* m_e}{h^{10}c^3} \left(k_{\mathrm{B}}T\right)^6 \Theta_{\mathrm{npe}} \\ \epsilon_0^{\mathrm{dUrca},\mu^-} &= \epsilon_0^{\mathrm{dUrca},e^-} \Theta_{\mathrm{np}\mu} \\ \epsilon_0^{\mathrm{dUrca,total}} &= \epsilon_0^{\mathrm{dUrca},e^-} + \epsilon_0^{\mathrm{dUrca},\mu^-},\end{aligned} \tag{9}$$

where we use the weak coupling constant $G_{\mathrm{F}} = 1.436 \times 10^{-62}\,\mathrm{Jm}^3$ and Cabibbo angle $\sin\theta_{\mathrm{C}} = 0.228$ (Zyla et al. 2020), and in-medium axial vector coupling constant from Carter & Prakash (2002), $g_{\mathrm{A}} = -1.2601(1 - \rho/(4.15(\rho_0+\rho))$. We account for in-medium interactions through m_x^*, which represents the Landau effective mass of species x. $\Theta_{\mathrm{npe}(\mu)}$ is a step function that restricts direct Urca reactions to the regions with $\rho > \rho_{\mathrm{dUrca}}$.

2.3. *Treatment of superfluidity and superconductivity*

Including superfluidity and superconductivity in the neutron star core model changes the neutrino luminosity, since the local neutrino emissivity is exponentially reduced by a reduction factor R_L, giving $\epsilon^{\mathrm{dUrca}} = \epsilon_0^{\mathrm{dUrca}} R_L$ (Yakovlev et al. 2001). We consider both proton singlet (PS) ($^1\mathrm{S}_0$) and neutron triplet (NT) ($^3\mathrm{P}_2$, $m_J = 0$) pairing in the core. For proton singlets, the reduction factor is given by (Yakovlev et al. 2001)

$$\begin{aligned}R_{\mathrm{L}} &= \left[0.2312 + \sqrt{(0.7688)^2 + (0.1438\ v_{\mathrm{S}})^2}\right]^{5.5} \\ &\quad \times \exp\left(3.427 - \sqrt{(3.427)^2 + v_{\mathrm{S}}^2}\right), \\ v_{\mathrm{S}} &= \sqrt{1-\tau}\left(1.456 - \frac{0.157}{\sqrt{\tau}} + \frac{1.764}{\tau}\right),\end{aligned} \tag{10}$$

while for neutron triplets,

$$\begin{aligned}R_{\mathrm{L}} &= \left[0.2546 + \sqrt{(0.7454)^2 + (0.1284\,v_{\mathrm{T}})^2}\right]^{5} \\ &\quad \times \exp\left(2.701 - \sqrt{(2.701)^2 + v_{\mathrm{T}}^2}\right), \\ v_{\mathrm{T}} &= \sqrt{1-\tau}\left(0.7893 + \frac{1.188}{\tau}\right).\end{aligned} \tag{11}$$

Here $\tau = T/T_c$, where T_c is the critical temperature, calculated according to each gap model parametrization, and T is the local temperature at radius r, $T(r) = \tilde{T}\exp(-\phi(r))$, with $\tilde{T}$ the temperature of the isothermal core as measured at infinity.

When proton singlet superconductivity and neutron triplet superfluidity are simultaneously active, we use the approximation

$$R_L \sim \min\left(R_{L,\mathrm{singlet}}, R_{L,\mathrm{triplet}}\right) \tag{12}$$

which is valid in the limit of strong superfluidity (Levenfish & Yakovlev 1994a). A more accurate calculation could be performed with combinations of the asymptotic expressions described in Levenfish & Yakovlev (1994a), however, since $T_c \gg T$ except in a narrow range of density, they would only provide minor corrections.

The heat capacity of neutrons and protons is similarly reduced when they are superfluid or superconducting, $\mathrm{C}_{p,n}^{\mathrm{superfluid}} = \mathrm{C}_{p,n}\, R_C$ (Levenfish & Yakovlev 1994b), where, for proton singlets,

$$\begin{aligned}R_C &= \left[0.4186 + \sqrt{(1.007)^2 + (0.5010\,u_{\mathrm{S}})^2}\right]^{2.5} \\ &\quad \times \exp\left(1.456 - \sqrt{(1.456)^2 + u_{\mathrm{S}}^2}\right), \\ u_{\mathrm{S}} &= \sqrt{1-\tau}(1.456 - 0.157/\sqrt{\tau} + 1.764/\tau),\end{aligned} \tag{13}$$

and for neutron triplets,

$$\begin{aligned}R_C &= \left[0.6893 + \sqrt{(0.790)^2 + (0.03983\,u_{\mathrm{T}})^2}\right]^{2} \\ &\quad \times \exp\left(1.934 - \sqrt{(1.934)^2 + \frac{u_{\mathrm{T}}^2}{16\pi}}\right), \\ u_{\mathrm{T}} &= \sqrt{1-\tau}(5.596 + 8.424/\tau).\end{aligned} \tag{14}$$

The total heat capacity is given by

$$C_{\mathrm{total}}^{\mathrm{core}} = \int_0^{R_{\mathrm{core}}} \frac{4\pi r^2 \sum C_x}{\left(1 - 2Gm(r)/c^2 r\right)^{1/2}}\, dr, \tag{15}$$

where C_x is the contribution to the local heat capacity from each particle species (Levenfish & Yakovlev 1994b),

$$C_x = \frac{m_x^* p_{F,x}}{3\hbar^3} k_B^2 T. \tag{16}$$

2.4. *Gap models*

To explore a range of different superfluid gap models, we use the analytic fits of Ho et al. (2015) (see their eq. [2] and Table II) to nine proton singlet (PS) and eight neutron triplet (NT) gap models. The PS gap models are AO (Amundsen & Østgaard 1985a), BCLL (Baldo et al. 1992), BS (Baldo & Schulze 2007), CCDK (Chen et al. 1993), CCYms/CCYps (Chao et al. 1972), EEHO (Elgarøy et al. 1996a), EEHOr (Elgarøy et al. 1996b), and T (Takatsuka 1973). The NT gap models are AO (Amundsen & Østgaard 1985b), BEEHS (Baldo et al. 1998), EEHO (Elgarøy et al. 1996c), EEHOr (Elgarøy et al. 1996b), SYHHP (Shternin et al. 2011), T (Takatsuka 1972), and TTav/TToa (Takatsuka & Tamagaki 2004). For additional references and details of the fits, see Ho et al. (2015). Unless it is clear from the context, we will prefix the gap name by either NT or PS to make

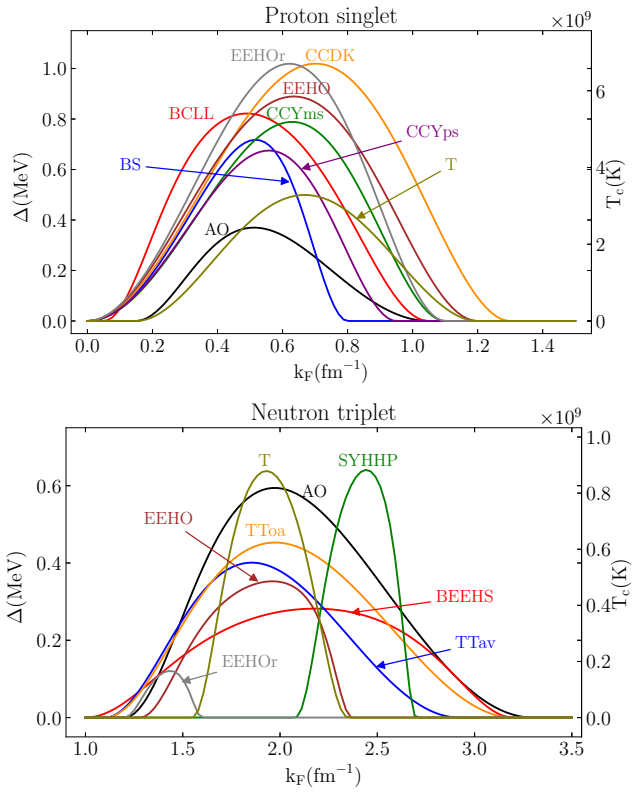

Figure 2. Superfluid gap Δ (MeV) and critical temperature T_c (K) as a function of Fermi momentum k_F (fm^{-1}) for proton singlet (top panel) and neutron triplet (bottom panel) gap models used in our calculations (see Ho et al. 2015 for details of the analytic fits and references for each gap model).

clear whether we are referring to a neutron triplet or proton singlet model, e.g. NT AO refers to the neutron triplet AO model.

Figure 2 shows these gap models as a function of k_F. To help characterize the region of the star which is superfluid, we define the opening $\rho_{\rm opening}$ and closing $\rho_{\rm closing}$ densities to correspond to the densities where the local temperature equals the critical temperature, $T_c = T(r)$. The opening and closing densities depend on the EOS (which maps k_F to density for each species), so we compute them for each neutron star model. Suppression of the dUrca emissivity will occur in the density range $\rho_{\rm opening} \lesssim \rho \lesssim \rho_{\rm closing}$. Our list of gap models covers a range of amplitudes and widths of the critical temperatures for nuclear pairings in neutron star cores, as well as early (low density) and late (high density) openings and closings, and so will allow us to explore the range of expected behavior.

3. MODELS OF MXB 1659-29 WITH DURCA NEUTRINO COOLING

In this section, we attempt to reproduce the observed neutrino luminosity of MXB 1659-29 with neutron star models in which the neutrino emission is by the nucleonic dUrca process, and considering different gap models for neutron and proton superfluidity. We start by considering models without superfluidity (§3.1), then consider the effect of neutron and proton pairing separately (§3.2) and in combination (§3.3).

Since the mass of the neutron star in MXB 1659-29 is unconstrained, we take the approach of calculating the range of allowed masses that are consistent with the observed neutrino luminosity L_ν^∞ of MXB 1659-29. We take the central value measured by Brown et al. (2018), $L_\nu^\infty = 3.9\times10^{34}$ erg/s, and also consider upper and lower values $L_\nu^\infty = 2\times10^{34}$ erg/s and $L_\nu^\infty = 7.8\times10^{34}$ erg/s which correspond approximately to the 1-σ range found by Brown et al. (2018) (see their Fig. 2). We also set the core temperature as observed at infinity to $\tilde{T} = 2.5\times10^7$ K (Brown et al. 2018) (note that $\tilde{T}$ is independent of radius in an isothermal star).

3.1. *Models with no pairing*

We first consider models without nuclear pairing, so that neutrino cooling occurs from all parts of the neutron star core where the density exceeds the dUrca threshold density. This situation is indicated schematically in Fig. 3a.

The top panel of Figure 4 shows the allowed masses for MXB 1659-29, i.e. the neutron star mass that has the same L_ν^∞ as MXB 1659-29, as a function of the slope of the symmetry energy L. The required mass decreases with L, and lies just above the dUrca threshold mass, shown as a dashed line in Figure 4. At the lowest values of L, we find $M \approx 1.8\ M_\odot$, whereas for $L \gtrsim 80$ MeV, the mass falls below 1.0 $M_\odot$. This result is a consequence of the high efficiency of dUrca processes which mean that only a small volume of the core is needed to supply the observed luminosity. The bottom panel of Figure 4 shows the volume fraction of the core involved in dUrca reactions, that is, the percentage of core volume above the dUrca threshold. For stars with the inferred luminosity, the dUrca volume fraction is around 1–4%, similar to the estimate of Brown et al. (2018).

Note that our solutions span a wide range of allowed neutron star masses. A common assumption is that only massive neutron stars can cool by dUrca reactions, but we see that for the EOS used here the threshold mass is small for high L values. For completeness, we show results for low neutron star masses $M < 1.0\,M_\odot$ even though these low masses are unlikely for astrophysical neutron stars (e.g. see Özel et al. 2012 for a discussion of the observed neutron star mass distribution). This im-

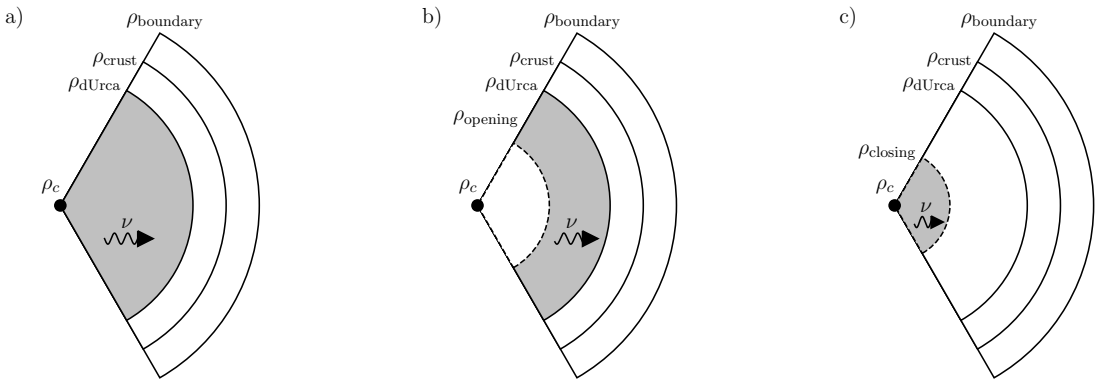

Figure 3. Three scenarios to explain the neutrino luminosity of MXB 1659-29. The shaded region indicates the part of the neutron star core undergoing active dUrca neutrino emission, indicated by the arrow. (a) No superfluidity in the region $\rho > \rho_{\rm dUrca}$. (b) A superfluid gap opens at a density $\rho_{\rm opening} > \rho_{\rm dUrca}$, suppressing dUrca in the centre and leading to neutrino emission from a shell. (c) The superfluid gap opens before the onset of dUrca, $\rho_{\rm opening} < \rho_{\rm dUrca}$, but closes again at high density $\rho_{\rm closing} < \rho_c$, where ρ_c is the central density. In this case neutrino emission is suppressed in the outer part of the core, reducing the size of the central emitting volume. Note that distances are not to scale in these diagrams; $\rho_{\rm boundary}$, $\rho_{\rm crust}$, and ρ_c represent the surface, crust-core boundary and central densities respectively. An example of case b (case c) is the $1.6\,{\rm M}_\odot$, $L = 70$ MeV ($2.01\,{\rm M}_\odot$, $L = 50$ MeV) star with the NT SYHHP gap shown in Fig. 5.

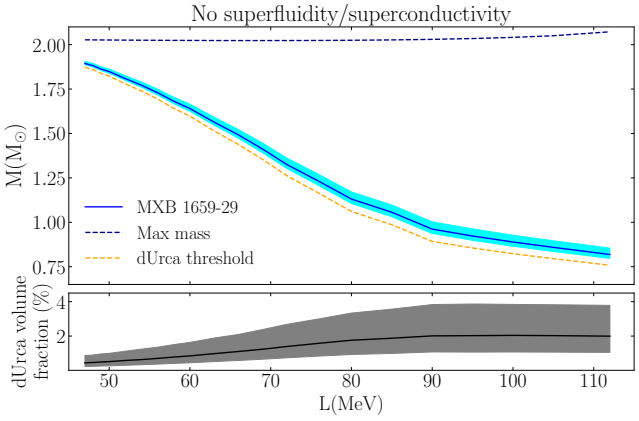

Figure 4. *Top panel:* Neutron star mass that reproduces the neutrino luminosity of MXB 1659-29 as a function of L for neutron star models without pairing. The blue shaded region corresponds to the 1σ uncertainty in neutrino luminosity from Brown et al. 2018. The dUrca threshold and maximum neutron star mass allowed by the EOS are shown by the dashed orange and dashed blue lines respectively. *Bottom panel:* Percentage of the core volume involved in unsuppressed dUrca reactions. The shaded region corresponds to the 1σ blue shaded region in the top panel.

plies that non-superfluid cores can explain MXB 1659-29 only if $L \lesssim 80$ MeV for the EOSs used here. A similar limit on L comes from the fact that some observed neutron stars are inconsistent with fast cooling (e.g. Wijnands et al. 2017), whereas our non-superfluid models predict that all neutron stars would have dUrca if L were larger than 80 MeV. However, these conclusions are relaxed when we include nuclear pairing, as we show in the next section.

3.2. *Effect of superfluidity*

We next include the reduction in neutrino emissivity due to nuclear pairing. By suppressing neutrino emission in regions of the core that are above the dUrca threshold density, superfluidity can lead to neutrino emission from either a reduced region of the core, or from a shell surrounding the superfluid core. These possibilities are shown schematically in Fig. 3b and c.

We first consider neutron and proton pairing separately to explore the role of each. The results are shown in Figure 5, where again we show the allowed neutron star mass as a function of L. The effects of nuclear pairing on the allowed masses are substantial, especially for neutron superfluidity. Due to the superfluid suppression of dUrca emissivity, the effective of onset of dUrca is delayed to higher density and the mass is increased in most cases (compare Fig. 4 and Fig. 5). In addition, for a given gap model, there is a wider range of inferred masses (a wider color band around the solid lines) than in the no pairing case, because superfluidity smooths the transition to dURCA emission, which means that L_ν^∞ increases more slowly with increasing M than in the no pairing case. Even though the NT critical temperatures are lower than PS, as shown in Fig. 2, neutron superfluidity has a larger effect on the required masses

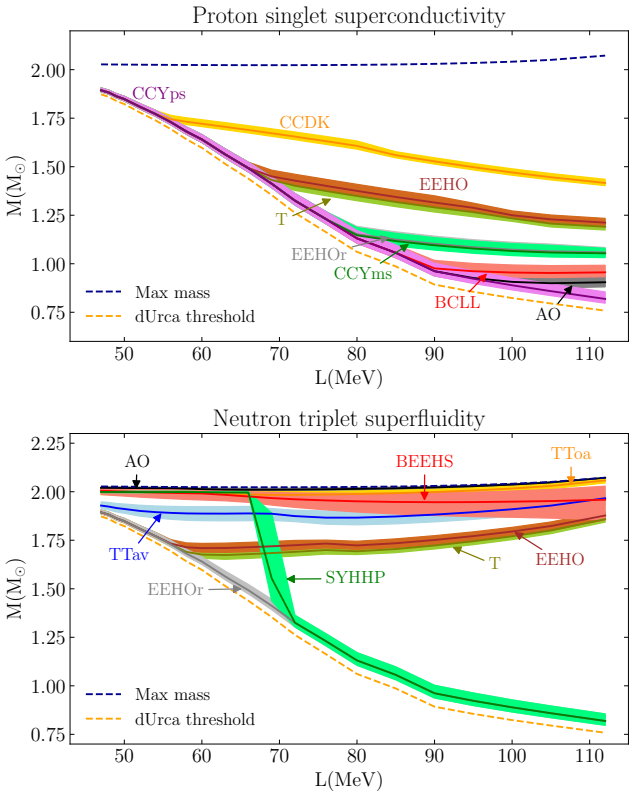

Figure 5. As Fig. 4, but including proton (top panel) and neutron (bottom panel) superfluidity. In the upper panel, the proton gap models BS and CCYps give the same results as the case with no-pairing shown in Fig. 4; we show only CCYps (in purple) in the Figure. In the lower panel, neutron gap model EEHOr (in grey) corresponds to the no-pairing curve shown in Fig. 4.

because the opening and closing densities for NT are more likely to occur in the region where dUrca reactions are allowed. Hence, in calculating L_ν^∞, the opening and closing densities and the width in density of a gap model is more important than its amplitude (as noted for example in the study of isolated cooling neutron stars by Beloin et al. 2018).

The ordering of the PS curves in the upper panel of Figure 5 follows the ordering of the gap closing density. For $L \leq 52$ MeV ($M \geq 1.75\,\mathrm{M}_\odot$), all the PS gaps close before the central density reaches the dUrca threshold and the PS gap results are the same as the no pairing results. Two PS gaps, BS and CCYps, close before the onset of dUrca for all L and hence give the same results as the no-pairing case. The other gaps predict increasing mass as the gap closing density increases: in order of increasing density, these are AO, BCLL, (CCYms,EEHOr), (T,EEHO), and CCDK. The pairs (CCYms, EEHOr) and (T,EEHO) have very similar gap closing densities (see Fig. 2) and therefore give

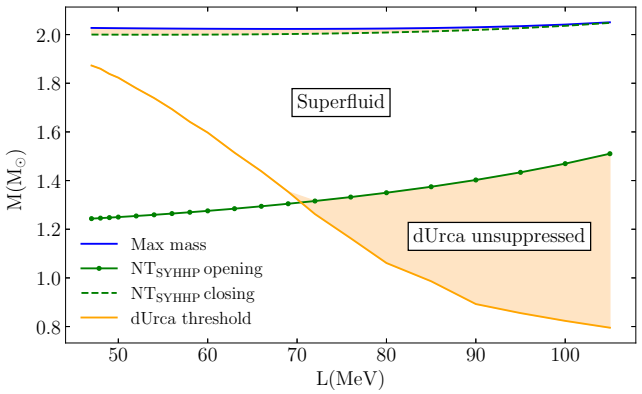

Figure 6. Masses of neutron stars that can cool by dUrca for the gap model NT SYHHP (shaded regions). dUrca is unsuppressed at low masses for $L \gtrsim 70$ MeV or at high masses close to the maximum mass. At intermediate masses, dUrca is quenched by superfluidity. We show the direct Urca threshold (orange curve), maximum mass (blue curve), and the opening (dotted green) and closing (dashed green) curves of NT SYHHP as a function of L.

very similar allowed mass ranges. So we see that the role of the PS gap is to delay the effective onset of dUrca to higher density (from $\rho_{\rm dUrca}$ to $\rho_{\rm closing}$) and therefore higher masses.

The NT gaps are more complicated because they have different orderings of $\rho_{\rm opening}$, $\rho_{\rm closing}$, relative to $\rho_{\rm dUrca}$. EEHOr has $\rho_{\rm closing} < \rho_{\rm dUrca}$ for all L and so gives the same results as the no pairing case. Apart from the gap SYHHP, which we discuss below, the curves again increase in mass following the ordering of the closing densities: (T,EEHO), TTav, BEEHS, TToa, AO, where again we bracket together T and EEHO which have similar closing densities and give similar mass constraints. Because the neutron gaps close at a much higher density than the proton gaps, the NT results for gaps that have $\rho_{\rm closing} > \rho_{\rm dUrca} > \rho_{\rm opening}$ give larger neutron star masses than the PS gaps: allowed masses are $\gtrsim 1.65$–$1.8\ M_\odot$, depending on L.

The gap model NY SYHHP is an interesting case. The distinct shape of this curve in Figure 5 is a direct consequence of the shape of this particular gap, which is narrow and peaks at higher density than the other NT gaps in Figure 2 (this gap model is a phenomenological model developed to fit the observed cooling of Cas A, see Shternin et al. 2011). In Figure 6, we show the regions of M and L where dUrca reactions are allowed somewhere in the neutron star core (orange shaded regions) or are suppressed by superfluidity (unshaded region). At large $L \gtrsim 70$ MeV, the NT SYHHP gap opens after the onset of dUrca reactions ($\rho_{\rm opening} > \rho_{\rm dUrca}$), leading to a range of masses $\lesssim 1.2$–$1.4\ M_\odot$ which cool by dUrca without any superfluid suppression. At smaller values of

$L \lesssim 70$ MeV, the core is superfluid already at the densities where dUrca reactions are allowed. Masses close to the maximum mass, however, have central densities that exceed the closing density of the gap $\rho_0 > \rho_{\rm closing}$, so dUrca reactions can then proceed. In Figure 5, where we are looking for solutions with a particular value of L_ν^∞, we see the transition from solutions at high L close to the dUrca threshold mass to solutions at low L close to the maximum mass. In the first case, the emission is from the core of the star that is not at high enough density to be superfluid; in the second case, the emission is from the core of the star which has a high enough density that the gap has closed.

We are able to find a solution that matches MXB 1659-29's neutrino luminosity except for one case, the largest $L = 112.7$ MeV in our EOS table with gap model NT AO. In this particular case, even a maximum mass star is not able to reproduce the upper value of L_ν^∞, although it can reproduce the central value. This result holds when we include proton superfluidity and NT AO neutron superfluidity together (§3.3); therefore the NT AO gap model at very large L's is disfavored. The reason for this is the very broad shape of the NT AO gap, as well as its large amplitude (Fig. 2 shows that AO, TToa and BEEHS all have roughly the same width but only AO fails to fit the data).

The introduction of pairing relaxes the conclusion from the no-pairing models that $L \gtrsim 80$ MeV requires low neutron star masses that are likely not realizable in nature. Once pairing is included, Figure 5 shows that the masses are significantly increased for many of the gap models. As mentioned above, the exceptions are the NT gaps EEHOr and SYHHP (which either close before or open after $\rho_{\rm dUrca}$, respectively), and the 4 PS gaps BCLL, AO, BS and CCYps (which close before $\rho_{\rm dUrca}$), which all allow solutions near the dUrca threshold.

3.3. *Combination of neutron and proton pairing*

We now include both proton and neutron pairing in the core. Three representative cases are shown in Figure 7. The top panel of Figure 7 shows the behavior that we find for most combinations of NT and PS pairings, namely that the neutron superfluid suppression dominates and the effect of proton superconductivity is negligible (a similar conclusion was reached by Han & Steiner 2017). This can be seen in the top panel of Figure 7, where the NT gap model alone produces the same result as the combination of NT and PS (in this case, the solutions are all near the maximum mass for the broad gap model NT AO). The reason that the proton gap does not change the results is that neutron superfluidity is usually active in larger volumes of the core of the neutron

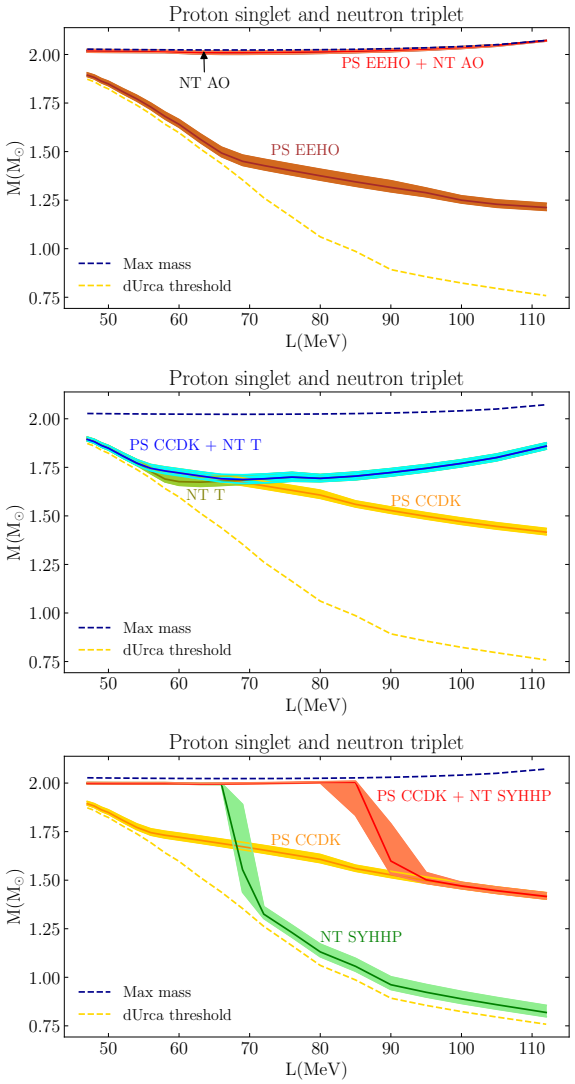

Figure 7. As Fig. 4, but for three examples of NT and PS combinations. In each case, we show the results with proton pairing only, neutron pairing only, and with both neutron and proton pairing included. *Top panel*: Gap models PS EEHO and NT AO. NT AO's curve is under the curve of the combination. *Middle panel*: Gap models PS CCDK and NT T. *Bottom panel*: Gap models PS CCDK and NT SYHHP.

star, despite its lower critical temperature, when compared with proton superconductivity gap models. In that case, we obtain the same results as before for the allowed range of inferred masses, $\approx$ 1–5%.

There are some pairings of PS and NT gaps, however, for which the choice of the proton pairing gap does change the results. In that case, the results from a model with both PS and NT gaps included can be quite different from those with neutron superfluidity only. Two examples are shown in the middle and bottom panels of Figure 7, both involving the PS CCDK

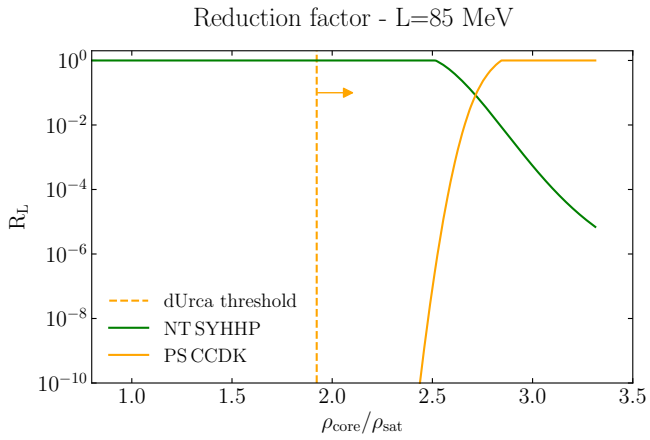

Figure 8. Reduction factor R_L of gap models PS CCDK and NT SYHHP as a function of core number density over saturation density, for a neutron star with $L = 85$ MeV and $M = 1.74\,M_\odot$. The vertical dotted line represents the dUrca threshold and the region to the right of it, indicated with the arrow, where dUrca reactions take place.

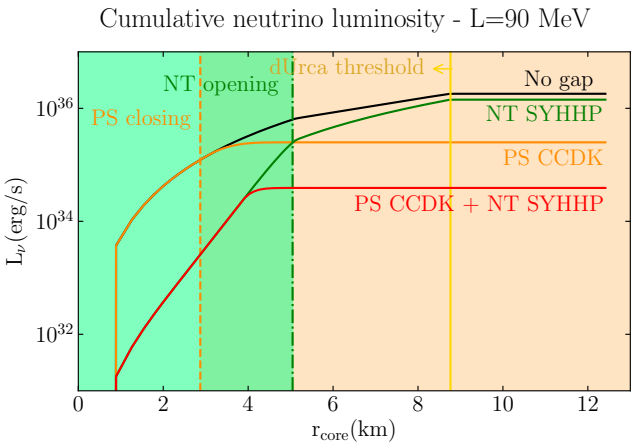

Figure 9. Cumulative dUrca neutrino luminosity as a function of radial distance, for a star with total mass $M = 1.60\,M_\odot$ and $L = 90$ MeV. We display the no gap case (black curve) along with the PS CCDK only case (orange curve), the NT SYHHP only case (green curve) and the PS CCDK + NT SYHHP combination (red curve). The region to the left of the vertical yellow line (dUrca threshold) represents the radii emitting dUrca neutrinos. The NT SYHHP opening curve is the dotted dashed green vertical line. The shaded areas are regions under superfluidity, detailed explanation in the text.

gap which extends to higher density than the other PS gaps (see Fig. 2). In the example in the middle panel, for $L \lesssim 70$ MeV, stars with the inferred luminosity have more of their core volume under PS CCDK pairing than under NT T pairing, thus their calculated neutrino luminosity versus mass curve reproduces the previously found PS CCDK curve. For $L \gtrsim 70$ MeV, NT T dominates instead and the L_ν^∞–M curve reproduces the NT T curve. Note that the width of the calculated mass curve remains narrow, indicating that the range of allowed masses of the star is still small.

In the lower panel of Figure 7, we show an example in which the solution transitions between NT-dominated high mass solutions (for $L \leq 80$ MeV) to PS-dominated intermediate mass solutions (for $L > 90$ MeV). The transition is significantly shifted in L compared to the NT calculation alone. Note that, at the transition, the range of inferred masses is considerably larger than before, up to $\approx 12\%$ variation in mass. The reason that the results for PS+NT are different from either PS or NT alone is that there are regions in the star where both proton and neutron superfluidity provide comparable suppression factors rather than one or the other dominating. Figure 8 shows a specific example of how the reduction factor R_L (see §2.3) varies with density for a star with mass 1.74 $M_\odot$ and for $L = 85$ MeV for this choice of gap models. This shows that the proton and neutron reduction rates become comparable at densities higher than the dUrca threshold, so that both play a role, suppressing emission over a large fraction of the core.

To show the different emission regions inside the star in more detail, Figure 9 shows the cumulative neutrino luminosity profile for a particular case from the lower panel of Figure 7 ($L = 90$ MeV and 1.6 $M_\odot$). The black curve shows the dUrca luminosity without any superfluidity; the other curves show how this is suppressed as superfluidity is introduced, either NT only, PS only, or NT+PS. The NT+PS curve follows the NT-only curve for the innermost ≈ 4 km, showing that the NT-pairing suppression dominates there. That region is within the green shaded area on the plot, corresponding to active neutron triplet pairing. At ≈ 5 km, that gap closes and the proton gap then dominates, represented by the pink shaded area. Its large reduction factor stops the luminosity from accumulating and the curve goes flat, such that the total luminosity is obtained at the innermost part of the core. Note that between 4 km and 5 km proton reduction rates dominate, even though both nucleon pairings are active. This shifting of neutron and proton superfluidity regions of influence is the signature of transitions as seen in the lower panel of Figure 7.

The fact that in most cases the neutron gap dominates over the proton gap (as in the top panel of Fig. 7) means that the number of NT and PS gap model combinations that predict low mass stars ($M \leq 1.0\,M_\odot$) at large L is actually small. Examples are PS EEHOr+NT SYHHP or PS CCYms+NT EEHOr, which have a late

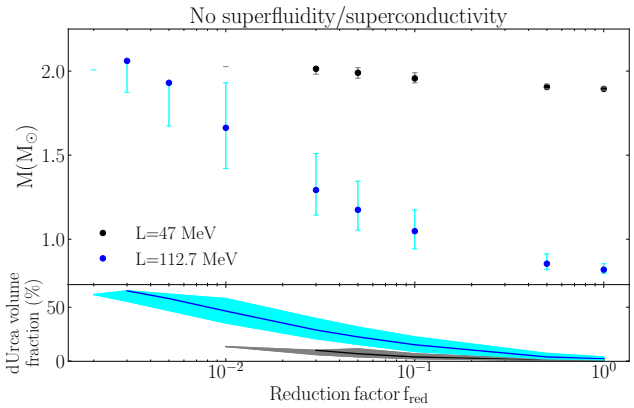

Figure 10. Neutron star mass that reproduces the neutrino luminosity of MXB 1659-29 (*top panel*), and the corresponding dUrca emission volume fraction (*bottom panel*), both as a function of the dUrca reduction factor $f_{\rm red}$ for neutron star models without pairing. The error bars in the top panel and the shaded region in the bottom panel correspond to the 1σ uncertainty in neutrino luminosity from Brown et al. 2018. We show results for $L = 47$ MeV (black) and $L = 112.7$ MeV (blue); results for intermediate values of L lie between these two curves.

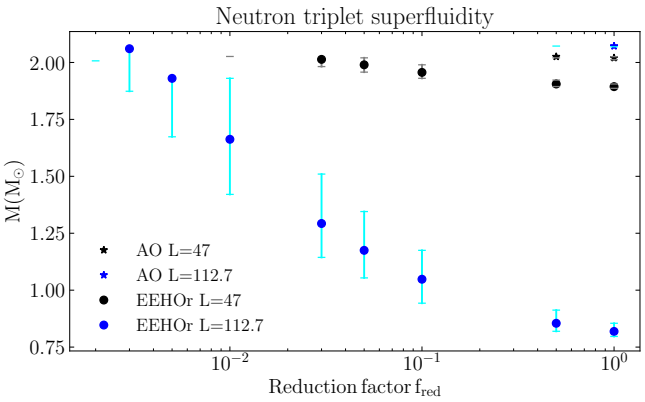

Figure 11. As Fig. 10, but including NT superfluidity. We show results for the strongest neutron triplet gap model NT AO (stars) and the weakest neutron triplet gap model NT EEHOr (circles).

opening of the NT gap or a weak NT superfluidity, respectively. Most of the nuclear pairing combinations investigated favor intermediate to high masses at large L. Furthermore, the range of allowed masses is consistently $\approx 5\%$ for most cases, so that even though superfluidity can change the density range in which significant dUrca cooling happens, the emitting volume is always a small fraction of the core volume.

4. REDUCED DURCA EMISSIVITY

The results of the previous section show that a wide range of models are compatible with the observed neutrino luminosity of MXB 1659-29. However, the high efficiency of the dUrca process means that only a small fraction of the neutron star core is emitting in these cases, and the required luminosity is obtained for only a narrow range of neutron star masses. In this section, we investigate how the emitting volume and range of allowed neutron star masses change if the dUrca emissivity is reduced by a constant reduction factor $f_{\rm red}$. For example, naively one might expect that taking $f_{\rm red} \sim 0.1$ would increase the emission volume from a few percent to tens of percent of the core, with a corresponding wider range of neutron star masses able to reproduce the observation of MXB 1659-29.

We do not have a specific physical model in mind for the reduction factor $f_{\rm red}$. This factor could model an uncertainty in the neutron and proton effective masses, simulating the emissivity (Eq. 9) for a different hadronic EOS, or it could mimic the behavior of other, less efficient, fast cooling dUrca reactions including other particles such as hyperons or Δ resonances. To consistently implement dUrca cooling from exotic particles would require that we update our EOS to account for the different particle content, and also adjust the dUrca threshold density accordingly. Here, as a first check on how our results might change with a less efficient process, we keep the same EOS and dUrca threshold but scale the nucleonic dUrca emissivity by the constant factor $f_{\rm red}$ everywhere in the star. Since a more exotic cooling process likely has a higher threshold density than dUrca, the neutrino luminosity we calculate here can be viewed as an approximate upper limit on the emissivity for that case.

Figure 10 shows the results for models with no pairing. We show the allowed neutron star mass as a function of $f_{\rm red}$ for two different values of L that span the range of our EOSs. Values of $f_{\rm red} \gtrsim 3 \times 10^{-2}$ are able to reproduce the source's most likely luminosity for all EOS. For the larger L case, even lower values of $f_{\rm red} \gtrsim 3 \times 10^{-3}$ are able to fit the data. Values of $f_{\rm red}$ smaller than these limits are not allowed because even the maximum mass neutron star is not able to provide sufficient neutrino luminosity. The reason that smaller values of $f_{\rm red}$ are allowed for larger L is that, as explained previously, larger L EOS have a lower dUrca threshold and a slightly larger maximum mass. Therefore, they have solutions in which a large fraction of the volume of the core is emitting neutrinos, as can be seen in the lower panel of Figure 10, and therefore can accommodate a small value of $f_{\rm red}$ while still producing the required luminosity.

Considering nuclear pairing, there is a similar tendency of larger L allowing smaller $f_{\rm red}$. As in the case of $f_{\rm red} = 1$, neutron triplet pairing dominates for most

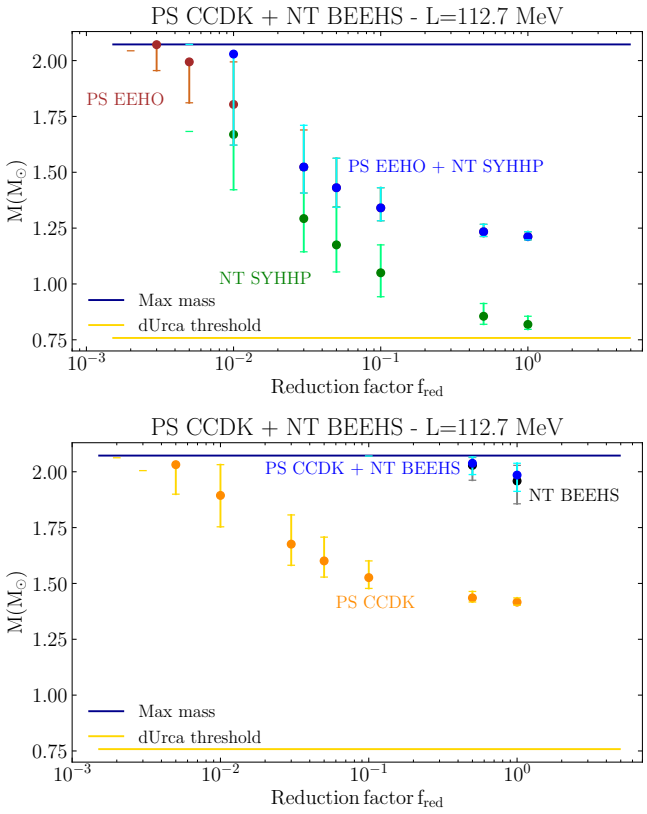

Figure 12. As Fig. 10, but for two different combinations of NT and PS superfluidity: PS EEHO+NT SYHHP (*top panel*) and PS CCDK+NT BEEHS (*bottom panel*). Horizontal lines represent the dUrca threshold (orange) and maximum mass (blue).

combinations of neutron and proton superfluidity, so that the calculated mass for the combination is the same as the triplet only mass calculations with different $f_{\rm red}$. In Figure 11, we show these results for the weakest and strongest NT gap models, for values of $L = 47$ MeV and $L = 112.7$ MeV that span the range of our EOSs (intermediate values of L lie between these curves). The results are quite similar to the no pairing models, except that the masses are increased to slightly higher values.

For a few combinations of gap models, proton pairing reduction rates become important. Two examples are shown in Figure 12. The top panel shows the case of PS EEHO + NT SYHHP. For large values of $f_{\rm red} \sim 1$, proton pairing dominates and the PS+NT result matches the PS-only result; for $f_{\rm red} \lesssim 10^{-2}$, neutron pairing dominates instead. Similarly to the discussion on the previous section, this effect is a feature of the competition of proton and neutron reduction rates. The role of the protons can be much larger for small $f_{\rm red}$ than for the $f_{\rm red} = 1$ case, since a larger core volume is active.

For the case illustrated in the top panel of Figure 12, the competition between the neutron and proton reduction rates results in a wider range of allowed masses for the combination PS EEHO + NT SYHHP when $f_{\rm red} \sim 10^{-2}$. Sometimes, however, as in the case shown in the bottom panel of Figure 12, that competition leads to a smaller range of masses. This happens because the total neutrino luminosity depends on the strength of the reduction rates as a function of the star's volume, so a pairing combination can lead to stronger or weaker overall luminosity suppression when compared with pure proton or neutron pairing, depending on the star's size and the gap model opening and closing curves. This counter-intuitive result can be more evident with a less efficient dUrca process (with $f_{\rm red} < 1$), which encompasses larger volumes actively emitting neutrinos hence potentially providing more room for different volumetric reduction rate distributions.

In summary, we find that we can reproduce the inferred luminosity of MXB 1659-29 for any combination of proton and neutron pairing and L as long as $f_{\rm red}$ is not too small. Typically, we need $f_{\rm red}$ larger than $\sim 3 \times 10^{-3} - 3 \times 10^{-2}$. In principle this constrains alternative fast neutrino emission mechanisms, e.g. from pions or kaons which could be suppressed relative to nucleonic dUrca by a factor of 1000 or more (Yakovlev et al. 2001). This suggests that it would be interesting to further explore models with alternative fast processes that incorporate consistent equations of state and dUrca thresholds. Two other considerations are that the allowed range of neutron star masses can be larger with $f_{\rm red} < 1$, making the model more likely to be able to explain the observations of MXB 1659-29, however this is not always the case. Furthermore, small values of $f_{\rm red}$ that result in most of the core volume emitting for MXB 1659-29 may fail to reproduce colder neutron stars, particularly for strong pairing combinations, such as PS CCDK+NT BEEHS or low values of L.

5. THE HEAT CAPACITY OF MXB 1659-29

In the previous sections we have shown that a variety of different models can account for the neutrino luminosity of MXB 1659-29. One way to distinguish these different models is through the heat capacity of the neutron star core, which depends on the degree of superfluidity (Brown et al. 2018). In this section, we calculate the total heat capacity of our solutions to quantify the nuclear pairing reductions.

In Figure 13, we show the total heat capacity of stars that match the neutrino luminosity of MXB 1659-29 with either no pairing or NT superfluidity only. The value of heat capacity depends primarily on the neutron

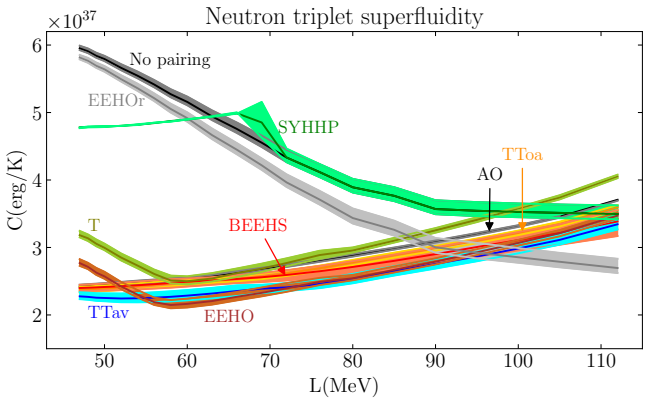

Figure 13. Neutron star heat capacity as a function of L for models that reproduce the observed neutrino luminosity of MXB 1659-29. The shaded regions around each curve correspond to the 1σ uncertainty in neutrino luminosity from Brown et al. 2018. We show results for no pairing and for different NT gap models.

star mass required to produce the observed neutrino luminosity (compare each gap model with the corresponding curves in the lower panel of Fig. 5). In some cases, such as the case with no or weak pairing, where the best fitting mass decreases with increasing L, the heat capacity decreases with L. In other cases with strong NT superfluid suppression, the allowed masses are larger and tend to increase with L; the heat capacity in those cases increases towards larger L.

Figure 14 shows the heat capacity as a function of the neutrino luminosity (following Cumming et al. 2017 and Brown et al. 2018) for different combinations of PS and NT gaps. Unlike neutrino luminosity, for which only the part of the core above the threshold density contributes, the entire volume of the core contributes to the heat capacity. Therefore the superfluid reduction to heat capacity is always visible, even for weak gap models. In addition, the heat capacities of stars with combined superconductivity and superfluidity are significantly smaller than when only one of these pairings is present. As shown in eqs. (13) and (14), the stronger the gap model, that is, the larger its critical temperature compared to the star's temperature, the smaller the star's total heat capacity. The combination of the weakest gap models, PS BS + NT EEHOr, is the closest heat capacity to the no-pairing case. The combination of the strongest ones, PS CCDK + NT AO, approaches the value of heat capacity coming from the leptons only (grey band), ie. close to full suppression of the nucleonic contribution to the heat capacity. Other gap models will generate stars with heat capacities between these two limits, as for the example shown of PS CCDK + NT SYHHP. The high efficiency of the dUrca process

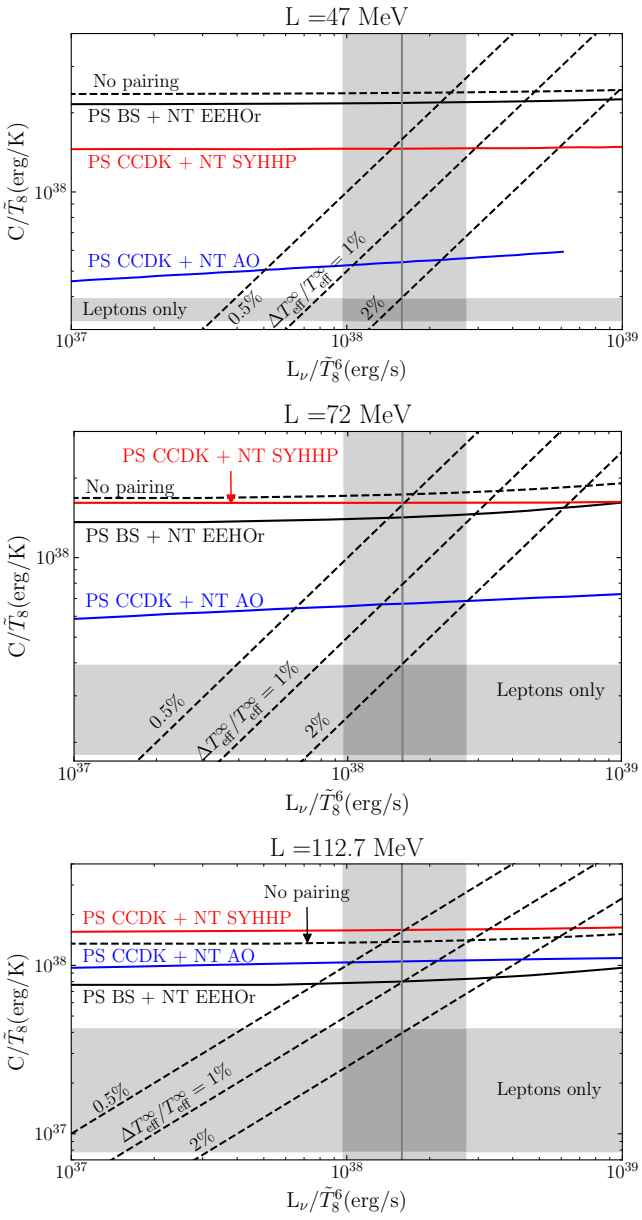

Figure 14. Heat capacity as a function of dUrca neutrino luminosity for neutron stars with different choices for NT and PS gaps. Models calculated for $L = 47$ MeV, $L = 72$ MeV and $L = 112.7$ MeV, respectively on the top, middle and bottom panels. We show results for no pairing (dashed curve) and for three combinations of NT and PS gaps as indicated (black, red and blue curves). The vertical gray area highlights the observed neutrino luminosity range for MXB 1659-29 from Brown et al. 2018. The horizontal gray area shows the contribution to the heat capacity from leptons. Diagonal dashed lines show the predicted surface temperature variation over a decade given the values of L_ν and C.

together with the small emitting volumes in the case of MXB 1659-29 lead to the very shallow gradient of the curves in Figure 14, i.e. the heat capacity is quite insensitive to L_ν^∞ since L_ν^∞ changes rapidly with neutron star mass.

The diagonal lines in Figure 14 show the variation in neutron star surface temperature that would be expected over a decade, given the neutrino cooling luminosity L_ν and the heat capacity C. To calculate those curves, we use equation (24) of Cumming et al. (2017), and following their work we assume that the change in core temperature $\tilde{T}$ is related to the change in effective (surface) temperature $T_{\rm eff}$ by $\Delta\tilde{T}/\tilde{T} \approx 1.8\,\Delta T_{\rm eff}^\infty/T_{\rm eff}^\infty$. Our results show that, because the different gap models span almost the full range of heat capacity between the unpaired and lepton-only values, constraints on $\Delta T_{\rm eff}^\infty/T_{\rm eff}^\infty$ at the percent level can discriminate between different gap models, clearly indicating whether MXB 1659-29 is strongly or weakly superfluid. This result, valid for all studied EOS, signals that future measurements of cooling in quiescence of MXB 1659-29 would constrain nuclear pairing in the neutron star core.

6. DISCUSSION

6.1. *Cooling of MXB 1659-29 by dUrca*

We find a range of models that reproduce the observed neutrino luminosity L_ν^∞ of MXB 1659-29 with dUrca neutrino emission. The predicted neutron star mass depends sensitively on the choice of L and gap model (Fig. 5). Since only a small volume of the core undergoing dUrca reactions is needed to explain the observed luminosity ($\approx$ 1–4% of the core volume), these solutions tend to lie close to either the mass where dUrca reactions first turn on, i.e. where the central density first exceeds the dUrca threshold, or the mass where superfluidity turns off, i.e. where the central density is large enough that the critical temperature T_c falls below the core temperature, quenching superfluidity and allowing dUrca reactions to proceed.

For our EOS, the dUrca threshold mass $M_{\rm dUrca}$ varies from $\approx$ 1.85 $M_\odot$ at $L \approx 50$ MeV to $\approx$ 1.1 $M_\odot$ at $L \approx 80$ MeV. In this range of L it is possible that the mass of MXB 1659-29 lies near $M_{\rm dUrca}$, and superfluidity is not needed. However, for $L \gtrsim 80$ MeV, $M_{\rm dUrca}$ drops below the smallest mass expected for astrophysical neutron stars, *i.e.* it becomes low enough that all observed neutron stars should be cooling by dUrca if they are not superfluid. In that case, suppression of dUrca by superfluidity is essential to allow a solution in which MXB 1659-29 lies just above the mass where dUrca cooling turns on (as well as providing a range of lower masses where neutron stars are able to cool by slow neutrino processes).

We find that neutron pairing plays a much more important role than proton pairing in moving the onset of dUrca cooling to larger masses. This is because the neutron triplet pairing occurs at a higher density than proton singlet (Fig. 2), and so is most likely the cause of superfluidity in the high density regions where dUrca operates. Proton gap models that close at high density can play a role, e.g. the CCDK model shown in Figure 2, particularly at intermediate values of $L \sim 60$–80 MeV. In cases where superfluidity moves the onset of dUrca cooling to higher masses, the predicted mass for MXB 1659-29 directly reflects the density at which the gap closes (Fig. 5).

We were able to find some combinations of gap models that could not explain MXB 1659-29 in the case where $L \gtrsim 80$ MeV. Two examples are the combinations PS EEHOr and NT SYHHP or PS CCYms and NT EEHOr. In these cases, the proton gap closes at low density, and the neutron gap is either very weak (in the case of NT EEHOr) or opens at higher density than other models (NT SYHHP), allowing a region of normal matter near the dUrca threshold, and giving a mass near the threshold mass, ie. $\lesssim 1\ M_\odot$. However, in the majority of cases using other gap combinations we found that superfluidity acts effectively to increase the predicted mass to values above $\approx$ 1.65–1.8 $M_\odot$ depending on L.

In some cases, the superfluid gap extends to high enough density that the predicted mass lies close to the maximum neutron star mass for any value of L. Particular examples are the neutron gap models NT AO, TToa, and BEEHS. In one case, with the NT gap AO (the gap with the broadest density range and largest amplitude) and the largest value of L in our EOS table, $L = 112.7$ MeV, we were not able to fit the 1σ upper limit on L_ν^∞. Even in other cases where we could fit MXB 1659-29 adequately with a mass close to the maximum mass, this could cause problems explaining colder sources that require even higher neutrino luminosities, since it does not leave much room to increase the mass and therefore neutrino luminosity further. In particular, the sources SAX J1808.4-3658 and 1H 1905+00 have quiescent luminosities significantly below MXB 1659-29 (e.g. see Fig. 3 of Potekhin et al. 2019). Indeed, Potekhin et al. (2019) found that a suppressed triplet pairing was necessary to explain SAX J1808.4-3658: their standard model of PS BS + NT BEEHS was not able to produce cold enough stars. In this sense MXB 1659-29, with its intermediate quiescent luminosity and small dUrca-active volume, is an interesting data point to add to SAX J1808.4-3658 and 1H 1905+00 when constraining dUrca emission

(e.g. the study of Han & Steiner 2017), since a combination of gap models that can match SAX J1808.4-3658 for example may not match MXB 1659-29, and vice versa. Note that while MXB 1659-29 has been included in studies of the population of accreting transients (e.g. Potekhin et al. 2019), the atmosphere is often assumed to have a heavy composition which is inconsistent with the cooling data (Brown et al. 2018).

An open question is the small range of allowed masses for MXB 1659-29 in our models. The modelling of Brown et al. (2018) gave an uncertainty of about a factor of 2 in the derived value of L_ν^∞. Since the emitting volume is small, this translates to a narrow range of allowed neutron star mass for any given choice of L and gap model. For the great majority of nuclear pairing combinations, we found a mass range of $\lesssim 5\%$. For some specific EOS and gap model combinations, we can have up to 10% mass change, however, these cases are limited to intermediate L where the dominant pairing transitions from neutron to proton (e.g. SYHHP gap in Fig. 5 lower panel). Given the small number of sources available, it is perhaps unlikely that we would catch MXB 1659-29 at a mass within a few percent of the threshold mass. Without detailed modelling of the evolutionary history, it is difficult to quantify this probability, but it provides motivation for considering a less efficient fast process that would result in a larger emission volume and therefore might give a more natural explanation.

6.2. *Alternative fast emission processes*

If particles other than neutrons, protons, electrons and muons are present in the neutron star core, other dUrca-like reactions, which result in fast-cooling processes, may be possible (Yakovlev et al. 2001). These processes have emissivities lower than the hadronic ones, so we mimic their effect by multiplying the hadronic emissivities by a factor $f_{\rm red} < 1$. Not considering consistently calculated EOS and finding the new dUrca thresholds for these processes is an oversimplification that grants us only upper limits in allowed $f_{\rm red}$, but we perform that calculation to check its effects on different values of L. Smaller $f_{\rm red}$ in this context also mimics the cooling calculations of other RMF EOS with same L but smaller values of effective masses. We found that less effective dUrca reactions, with as low as 3% of the original emissivity for large L, can reproduce the inferred luminosity in heavier stars, but, at least in this simplified framework, are not necessarily favored. Considering again that much lower luminosities must be achievable, we predict that some EOS would have difficulty fitting that data with less effective emissivities, which is particularly evident when nuclear pairing is considered. Smaller reductions in emissivities can, in most cases, fit the data, except for strong neutron triplet pairing (NT AO, NT TToa, NT BEEHS), with any combination of proton superconductivity models.

Whenever hadronic and non-hadronic dUrca reactions occur simultaneously, hadronic emissivity dominates. Hence, dUrca reactions fueled by exotic particles could change the results presented here if their threshold happens before the hadronic dUrca threshold. Within our framework, this scenario would most likely disfavor exotic particles in large L EOS, by demanding their presence at too low densities. However, in consistently calculated exotic EOS the proton fractions used here to calculate the threshold could change dramatically, so one needs to verify this claim case-by-case for each EOS. Furthermore, other cooling processes not investigated here could be relevant in non-hadronic cold neutron stars and their contribution must be investigated, with special attention to in-medium effects.

6.3. *Future observational and experimental constraints*

Our calculations of the neutron star total heat capacity, combined with its inferred luminosity, have shown that a future measurement of temperature variation in a long time interval could help discriminate between core nuclear pairing models. Figure 14 shows that our models span the full range of heat capacity, from close to the minimal heat capacity where leptons only contribute, to the larger values where the nucleons in the core are unpaired. A precise measurement of that temperature variation, of a few percent, will exclude strong or weak combinations of pairing models, helping to determine the state of matter in the neutron star core. Achieving these observations requires sensitive X-ray observations over many years, and also requires that the source remain in quiescence for this long. MXB 1659-29 is promising for this, with a mean outburst rate of about 1 every 14 years so far (Maccarone et al. 2022).

We have taken M and L to be free parameters, but our results show that constraints on L and M from future experiments and observations would be extremely constraining for cooling models. For example, if it was shown experimentally that $L \gtrsim 80$ MeV, certain gap model combinations would immediately be ruled out for MXB 1659-29 in the context of our EOS, i.e. we need the gap to close at high enough density that the transition to dUrca is delayed.

The mass of the neutron star in MXB 1659-29 is currently unconstrained. Ponti et al. (2018) discuss the possibility of measuring the neutron star mass in MXB 1659-29 using X-ray spectroscopy of the inner regions of the accretion disk. They find that a mass mea-

surement with an uncertainty of about 5% may be possible with the next generation X-ray telescopes such as Athena (e.g. Nandra et al. 2013). Another possibility is to use spectral fitting of the neutron star thermal spectrum, either in quiescence or during Type I X-ray bursts, to infer constraints on mass and radius, although these methods currently have significant systematic uncertainties (Özel & Freire 2016). The thermal relaxation of the neutron star crust after accretion outbursts also depends on M, primarily through its effect on the crust thickness (Brown & Cumming 2009). In combination with a determination of the neutron star radius, this could lead to tighter constraints on the mass. Comparing the radius range $\approx$ 11.5–13 km recently inferred by Raaijmakers et al. (2021) from a variety of astrophysical data, including from NICER (Riley et al. 2021), with Figure 14 of Brown & Cumming (2009) suggests $M \lesssim 1.6\ M_\odot$ for MXB 1659-29. For the EOS studied here, this would require $L \gtrsim 60$ MeV and pairing strong enough to delay the onset of dUrca to this mass (see Figs. 5 and 7).

There are various experimental and astrophysical constraints on the value of the slope of the symmetry energy as summarized in Li & Han (2013). While several experimental results point toward a smaller value of the slope in the range of 40 to 60 MeV (Lattimer 2012; Drischler et al. 2020), recent experimental measurements on the neutron skin thickness of ^{208}Pb (Adhikari et al. 2021) implies that L can be much larger, $L = 106 \pm 37$ MeV (Reed et al. 2021). On the other hand, a very small neutron skin of ^{48}Ca was measured recently that suggests the L-value to be much smaller than all previous constraints combined (Zhang & Chen 2022). While challenging, there are future prospects of a more precise electroweak determination of the neutron skin at the future Mainz Energy-recovery Superconducting Accelerator (MESA) (Becker et al. 2018) that should allow to constrain L more stringently. From the astrophysical side, the prospects of measuring the radius of a neutron star and its tidal deformability that are both very sensitive to the L value have never been better. NICER aims to measure the neutron star radii with known masses, at a 3% level which should significantly constrain the value of L (Miller 2016). Moreover, future gravitational wave data from binary neutron star mergers should give a strong constraint on the tidal deformability that in turn will constrain L (Fattoyev et al. 2018).

ACKNOWLEDGEMENTS

We thank David Blaschke, Sangyong Jeon, Jérôme Margueron and Adriana Raduta for useful discussions and comments, and Ed Brown, Chuck Horowitz, Dany Page, and Sanjay Reddy for many conversations about transient LMXBs and MXB 1659-29 in particular. This work is supported in part by the Natural Sciences and Engineering Research Council of Canada (NSERC). MM is supported by the Schlumberger Foundation through a Faculty for the Future Fellowship. AC is a member of the Centre de Recherche en Astrophysique du Québec (CRAQ). FF is supported by the Summer Grant from the Office of the Executive Vice President and Provost of Manhattan College. Computations were made on the Beluga supercomputer at McGill University, managed by Calcul Quebec and Compute Canada.

Software: This work made use of the Python libraries Matplotlib (Hunter 2007), NumPy (Harris et al. 2020) and SciPy (Virtanen et al. 2020).

REFERENCES

Abbott, B. P., et al. 2017, Phys. Rev. Lett., 119, 161101, doi: https://doi.org/10.1103/PhysRevLett.119.161101

—. 2018, Phys. Rev. Lett., 121, 161101, doi: https://doi.org/10.1103/PhysRevLett.121.161101

Adhikari, D., et al. 2021, Phys. Rev. Lett., 126, 172502, doi: https://doi.org/10.1103/PhysRevLett.126.172502

Amundsen, L., & Østgaard, E. 1985a, Nuclear Physics A, 437, 487, doi: https://doi.org/10.1016/S0375-9474(85)90103-4

—. 1985b, Nuclear Physics A, 442, 163, doi: https://doi.org/10.1016/0375-9474(85)90140-X

Baldo, M., Cugnon, J., Lejeune, A., & Lombardo, U. 1992, Nuclear Physics A, 536, 349, doi: https://doi.org/10.1016/0375-9474(92)90387-Y

Baldo, M., Elgarøy, O., Engvik, L., Hjorth-Jensen, M., & Schulze, H.-J. 1998, Phys. Rev. C, 58, 1921, doi: 10.1103/PhysRevC.58.1921

Baldo, M., & Schulze, H.-J. 2007, Phys. Rev. C, 75, 025802, doi: 10.1103/PhysRevC.75.025802

Baym, G., Pethick, C., & Sutherland, P. 1971, Astrophys. J., 170, 299, doi: https://doi.org/10.1086/151216

Becker, D., et al. 2018, Eur. Phys. J. A, 54, 208, doi: 10.1140/epja/i2018-12611-6

Beloin, S., Han, S., Steiner, A. W., & Page, D. 2018, Phys. Rev. C, 97, 015804, doi: 10.1103/PhysRevC.97.015804

Beznogov, M. V., & Yakovlev, D. G. 2015a, MNRAS, 447, 1598, doi: 10.1093/mnras/stu2506

—. 2015b, MNRAS, 452, 540, doi: 10.1093/mnras/stv1293

Brown, E. F., & Cumming, A. 2009, ApJ, 698, 1020, doi: 10.1088/0004-637X/698/2/1020

Brown, E. F., Cumming, A., Fattoyev, F. J., et al. 2018, Phys. Rev. Lett., 120, 182701, doi: 10.1103/PhysRevLett.120.182701

Cackett, E. M., Wijnands, R., Linares, M., et al. 2006, MNRAS, 372, 479, doi: 10.1111/j.1365-2966.2006.10895.x

Carter, G., & Prakash, M. 2002, Physics Letters B, 525, 249, doi: https://doi.org/10.1016/S0370-2693(01)01452-6

Chao, N.-C., Clark, J., & Yang, C.-H. 1972, Nuclear Physics A, 179, 320, doi: https://doi.org/10.1016/0375-9474(72)90373-9

Chen, J., Clark, J., Davé, R., & Khodel, V. 1993, Nuclear Physics A, 555, 59, doi: https://doi.org/10.1016/0375-9474(93)90314-N

Chen, W.-C., & Piekarewicz, J. 2014, Phys. Rev. C, 90, 044305, doi: https://doi.org/10.1103/PhysRevC.90.044305

Cromartie, H. T., et al. 2019, Nature Astron., 4, 72, doi: 10.1038/s41550-019-0880-2

Cumming, A., Brown, E. F., Fattoyev, F. J., et al. 2017, Phys. Rev. C, 95, 025806, doi: https://doi.org/10.1103/PhysRevC.95.025806

Degenaar, N., Page, D., van den Eijnden, J., et al. 2021, MNRAS, 508, 882, doi: 10.1093/mnras/stab2202

Drischler, C., Furnstahl, R. J., Melendez, J. A., & Phillips, D. R. 2020, Phys. Rev. Lett., 125, 202702, doi: 10.1103/PhysRevLett.125.202702

Elgarøy, O., Engvik, L., Hjorth-Jensen, M., & Osnes, E. 1996a, Nuclear Physics A, 604, 466, doi: https://doi.org/10.1016/0375-9474(96)00152-2

—. 1996b, Phys. Rev. Lett., 77, 1428, doi: 10.1103/PhysRevLett.77.1428

—. 1996c, Nuclear Physics A, 607, 425, doi: https://doi.org/10.1016/0375-9474(96)00217-5

Fattoyev, F. J., Piekarewicz, J., & Horowitz, C. J. 2018, Phys. Rev. Lett., 120, 172702, doi: 10.1103/PhysRevLett.120.172702

Han, S., & Steiner, A. W. 2017, PhRvC, 96, 035802, doi: 10.1103/PhysRevC.96.035802

Harris, C. R., Millman, K. J., van der Walt, S. J., et al. 2020, Nature, 585, 357, doi: 10.1038/s41586-020-2649-2

Heinke, C. O., Jonker, P. G., Wijnands, R., Deloye, C. J., & Taam, R. E. 2009, ApJ, 691, 1035, doi: 10.1088/0004-637X/691/2/1035

Heinke, C. O., Jonker, P. G., Wijnands, R., & Taam, R. E. 2007, ApJ, 660, 1424, doi: 10.1086/513140

Ho, W. C. G., Elshamouty, K. G., Heinke, C. O., & Potekhin, A. Y. 2015, Phys. Rev. C: Nucl. Phys., 91, 015806, doi: https://doi.org/10.1103/PhysRevC.91.015806

Hunter, J. D. 2007, Computing in Science & Engineering, 9, 90, doi: 10.1109/MCSE.2007.55

Lattimer, J. M. 2012, Ann. Rev. Nucl. Part. Sci., 62, 485, doi: 10.1146/annurev-nucl-102711-095018

Lattimer, J. M. 2018, Physics Online Journal, 11, 42, doi: https://doi.org/10.1103/Physics.11.42

Lattimer, J. M., Pethick, C. J., Prakash, M., & Haensel, P. 1991, PhRvL, 66, 2701, doi: 10.1103/PhysRevLett.66.2701

Levenfish, K., & Yakovlev, D. G. 1994a, Astronomy Letters, 20, 43

—. 1994b, Astronomy Reports, 38, 247

Levenfish, K. P., & Haensel, P. 2007, Ap&SS, 308, 457, doi: 10.1007/s10509-007-9382-2

Li, B.-A., & Han, X. 2013, Phys. Lett. B, 727, 276, doi: 10.1016/j.physletb.2013.10.006

Maccarone, T. J., Degenaar, N., Tetarenko, B. E., et al. 2022, Monthly Notices of the Royal Astronomical Society, 512, 2365, doi: 10.1093/mnras/stac506

Mendes, M., Fattoyev, F. J., Cumming, A., & Gale, C. 2021, in Proceedings of the Sixteenth Marcel Grossmann Meeting on General Relativity, ed. G. Vereshchagin & R. Ruffini (Rome, Italy: World Scientific), doi: 10.48550/arXiv.2110.11077

Miller, M. C. 2016, Astrophys. J., 822, 27, doi: 10.3847/0004-637X/822/1/27

Miller, M. C., et al. 2019, Astrophys. J. Lett., 887, L24, doi: https://doi.org/10.3847/2041-8213/ab50c5

Miller, M. C., Lamb, F. K., Dittmann, A. J., et al. 2021, The Astrophysical Journal Letters, 918, L28, doi: 10.3847/2041-8213/ac089b

Nandra, K., Barret, D., Barcons, X., et al. 2013, The Hot and Energetic Universe: A White Paper presenting the science theme motivating the Athena+ mission, arXiv, doi: 10.48550/ARXIV.1306.2307

Negele, J., & Vautherin, D. 1973, Nucl. Phys. A, 207, 298, doi: https://doi.org/10.1016/0375-9474(73)90349-7

Özel, F., & Freire, P. 2016, ARA&A, 54, 401, doi: 10.1146/annurev-astro-081915-023322

Özel, F., Psaltis, D., Narayan, R., & Santos Villarreal, A. 2012, ApJ, 757, 55, doi: 10.1088/0004-637X/757/1/55

Page, D., & Reddy, S. 2012, Neutron Star Crust, Space Science, Exploration and Policies Series (Nova Science Publishers, Inc.). https://ui.adsabs.harvard.edu/abs/2012arXiv1201.5602P

Parikh, A. S., Wijnands, R., Ootes, L. S., et al. 2019, A&A, 624, A84, doi: 10.1051/0004-6361/201834412

Piekarewicz, J., & Centelles, M. 2009, Phys. Rev. C, 79, 054311, doi: https://doi.org/10.1103/PhysRevC.79.054311

Ponti, G., Bianchi, S., Muñoz-Darias, T., & Nandra, K. 2018, MNRAS, 481, L94, doi: 10.1093/mnrasl/sly120

Potekhin, A. Y., Chugunov, A. I., & Chabrier, G. 2019, A&A, 629, A88, doi: 10.1051/0004-6361/201936003

Raaijmakers, G., Greif, S. K., Hebeler, K., et al. 2021, ApJL, 918, L29, doi: 10.3847/2041-8213/ac089a

Reed, B. T., Fattoyev, F. J., Horowitz, C. J., & Piekarewicz, J. 2021, Phys. Rev. Lett., 126, 172503, doi: 10.1103/PhysRevLett.126.172503

Riley, T. E., et al. 2019, Astrophys. J. Lett., 887, L21, doi: https://doi.org/10.3847/2041-8213/ab481c

Riley, T. E., Watts, A. L., Ray, P. S., et al. 2021, ApJL, 918, L27, doi: 10.3847/2041-8213/ac0a81

Shternin, P. S., Yakovlev, D. G., Haensel, P., & Potekhin, A. Y. 2007, MNRAS, 382, L43, doi: 10.1111/j.1745-3933.2007.00386.x

Shternin, P. S., Yakovlev, D. G., Heinke, C. O., Ho, W. C. G., & Patnaude, D. J. 2011, Monthly Notices of the Royal Astronomical Society: Letters, 412, L108, doi: 10.1111/j.1745-3933.2011.01015.x

Takatsuka, T. 1972, Progress of Theoretical Physics, 48, 1517, doi: 10.1143/PTP.48.1517

—. 1973, Progress of Theoretical Physics, 50, 1754, doi: 10.1143/PTP.50.1754

Takatsuka, T., & Tamagaki, R. 2004, Progress of Theoretical Physics, 112, 37, doi: 10.1143/PTP.112.37

Virtanen, P., Gommers, R., Oliphant, T. E., et al. 2020, Nature Methods, 17, 261, doi: 10.1038/s41592-019-0686-2

Wijnands, R., Degenaar, N., & Page, D. 2013, MNRAS, 432, 2366, doi: 10.1093/mnras/stt599

—. 2017, J. Astrophys. Astron., 38, 49, doi: https://doi.org/10.1007/s12036-017-9466-5

Yakovlev, D. G., Kaminker, A. D., Gnedin, O. Y., & Haensel, P. 2001, Phys. Rep., 354, 1, doi: https://doi.org/10.1016/S0370-1573(00)00131-9

Yakovlev, D. G., & Pethick, C. J. 2004, ARA&A, 42, 169, doi: 10.1146/annurev.astro.42.053102.134013

Zhang, Z., & Chen, L.-W. 2022. https://arxiv.org/abs/2207.03328

Zyla, P. A., Barnett, R. M., Beringer, J., et al. 2020, Progress of Theoretical and Experimental Physics, 2020, doi: 10.1093/ptep/ptaa104